Aalborg Universitet

AALBORG UNIVERSITY

DENMARK

Modeling outdoor thermal comfort using satellite imagery

A principle component analysis-based approach

Mijani, Naeim; Alavipanah, Seyed Kazem; Firozjaei, Mohammad Karimi; Arsanjani, Jamal Jokar; Hamzeh, Saeid; Weng, Qihao

Link to publication from Aalborg University

Modeling outdoor thermal comfort using satellite imagery: A principle component analysis-based approach

Naeim Mijani[a], Seyed Kazem Alavipanah[a], Mohammad Karimi Firozjaei[a], Jamal Jokar Arsanjani[b], Saeid Hamzeh[a], Qihao Weng[c],*

[a] *Department of Remote Sensing and GIS, Faculty of Geography, University of Tehran, Tehran, Iran*
[b] *Geoinformatics Research Group, Department of Planning and Development, Aalborg University Copenhagen, A.C Meyers Vænge 15, DK-2450 Copenhagen, Denmark*
[c] *Center for Urban and Environmental Change, Department of Earth and Environmental Systems, Indiana State University, Terre Haute, IN 47809, USA*

ABSTRACT

A harmful effect of anthropogenic activities in urban environments is the increases of thermal discomfort and subsequently, a negative effect on humans' mental and physical performance. Therefore, it is of high importance to detect, monitor, and predict thermal discomfort, especially its temporal and spatial patterns in cities. The objective of this study is to propose a new method for modeling outdoor thermal comfort based on remote sensing and climatic datasets. To do so, several datasets were utilized, including those from Landsat, Moderate Resolution Imaging Spectroradiometer (MODIS), Digital Elevation Model (DEM) from Advanced Spaceborne Thermal Emission and Reflection Radiometer (ASTER), and climatic datasets from local meteorological stations. The method was experimented in the city of Tehran, Iran. For modeling outdoor thermal comfort, the Least Squares Adjustment (LSA) model was presented based on the Principle Component Analysis (PCA). In this model, the Principle Components (PCs) of the environmental and surface biophysical parameters were considered as independent variables and Discomfort Index (DI) as dependent variable. Finally, by determining the optimal values of the adjustment coefficients for each independent variable, maps of outdoor thermal comfort at different timestamps were produced and analyzed. The results of the modeling showed that correlation coefficient and Root Mean Square Error (RMSE) between the modeled and observed outdoor thermal comfort values at the meteorological stations for the training data sets were 0.86 and 1.80, for the testing data set were 0.89 and 2.04, respectively, while it was 0.85 and 1.15 for the self-deployed devices. The average values of DI in warm season of year was 8.5 °C higher than the cold season of the year. Further, in both warm and cold seasons of year the mean value of DI for bare land was found higher than other land covers, whereas that of water bodies lower than others. Our findings suggest that efficiency can be achieved for modeling outdoor thermal comfort using LSA with remote sensing and climatic datasets.

1. Introduction

Over the past decades, physical development of cities has caused many changes including land use and land cover changes, increased various types of pollutions, and climate changes (Brunsell 2006, Firozjaei et al. 2019b, Firozjaei et al. 2019d). Urbanization leads to changes of the natural landscape to artificial surfaces, hydrological cycle and surface biophysical properties (Panah et al. 2017, Silva et al. 2018, Firozjaei et al. 2020a). Among the most important adverse impacts of increased human activities is decreasing vegetation cover and increasing impervious surfaces that cause alter air and surface temperature, and surface energy balance (Senanayake et al. 2013, Cai et al. 2019, Firozjaei et al. 2020b). One of the most important effects of increased human activities and urban warming is the increase of thermal discomfort in urban environments (Liu et al. 2018, Musse et al. 2018).

Thermal comfort indicates the relationship between the impact of climate changes and the various dimensions of human life in urban environments. Outdoor thermal comfort is a condition of mind that expresses the satisfaction of the surrounding thermal environment (Choi and Yeom 2019, Hami et al. 2019). Outdoor thermal discomfort (even, stress) has different negative effects on various aspects of human

life, including social, economic, health and environmental aspects. Due to the prediction of increasing population growth and physical expansion of cities all over the world in the coming decades, it is of great importance to assess, monitor and predict the spatial and temporal patterns of outdoor thermal comfort in urban environments (Mijani et al. 2019).

Several studies have been conducted for modeling outdoor thermal comfort in urban environments based on synoptic station data (Van Hove et al. 2015, Katavoutas et al. 2016, Qaid et al. 2016, Morris et al. 2017). The spatial resolution of these data is inappropriate. Due to the spatial heterogeneity of the outdoor thermal comfort conditions in urban areas (Mushore et al. 2018), the synoptic station data alone does not have proper function for accurate modeling of the thermal and comfort changes in space and time. Previous studies have shown that outdoor thermal comfort in an area is affected by environmental and surface biophysical parameters (Tsunematsu et al. 2016, Xu et al. 2017, Mushore et al. 2018, Song and Wu 2018). Mijani et al. (2019) showed that outdoor thermal comfort in an urban area can be affected by downward surface shortwave and longwave radiation, surface upward longwave radiation, brightness, greenness and wetness of the surface. With the capabilities of remote sensing data for modeling environmental and surface biophysical parameters at different spatial and temporal resolutions, there is a high potential for using these data to model outdoor thermal comfort patterns and changes (Xu et al. 2017, Mushore et al. 2018, Mijani et al. 2019). Sobrino et al. (2013) investigated the outdoor thermal comfort condition in Madrid city, Spain, using thermal remote sensing and climatic data set at the meteorological stations. Discomfort Index (DI) was developed to model outdoor thermal comfort. Xu et al. (2017) applied humidity and air temperature data in ground stations and satellite images of Landsat and Sentinel for the production of outdoor thermal comfort maps in Fuzhou, China. The result showed that the outdoor thermal comfort was found in direct relation with the built-up index and inversely related with the vegetation cover and water body indexes. Song and Wu (2018) investigated the state of Wisconsin's outdoor thermal comfort in the United States based on the remote sensing data. Data sets from ground stations and images and products of the Moderate Resolution Imaging Spectroradiometer (MODIS) sensor were used. The results showed that land surface temperature (LST) had a greater effect on outdoor thermal comfort than built-up and vegetation covers. Mushore et al. (2018) studied outdoor thermal comfort in Zimbabwe in different seasons and land covers. Relative humidity and air temperature data recorded at ground stations and Landsat satellite images were used. It showed that Landsat 8 imagery had a high ability for modeling outdoor thermal comfort in different seasonal conditions. Ziaul and Pal (2019) analyze the patterns and changes of thermal comfort in different seasons in the English Municipality of Bazar (India) and its surrounding. The DI value was modeled based on the thermal bands of Landsat imagery and field observation data. The RayMan model was applied to calculate the Physiological Equivalent Temperature (PET) value. The results indicated that the extension discomfort zone in each season of 2016 significantly increased compare to 2010. In summer, extreme heat stress is experienced except the area under vegetation cover and water body. Lai et al. (2019) investigated the heat mitigating strategies to improve the outdoor thermal condition. In they study, the cooling effects of various strategies, including cool surface, vegetation cover, urban geometry, and water bodies was analyzed. They findings showed that urban geometry has the greatest effect on thermal comfort in summer followed by vegetation cover and water bodies. However, reflective surface led to the increased the amount of PET in summer. Arghavani et al. (2020) studied the effectiveness of different urban green strategies on the diurnal variability of urban heat island (UHI) and outdoor thermal comfort in Tehran Metropolis. In this study, satellite images of Landsat 8 and Sentinel-2 applied to calculated the urban density and fraction vegetation cover. Also, THI, ETI and RSI indices were calculated for assessing thermal comfort variations. They

results showed that in low-intensity residential area, diurnal cooling effects in all strategies (surface vegetation, green roof, surface vegetation/green roof) are simulated, while in high-intensity residential and commercial and industrial areas, daytime cooling is predicted. Over the city, surface vegetation has the least diurnal averaged cooling effects in comparison to the green roof approach. Also, the effect of its warming nighttime is more significant than the green roof. Feng et al. (2020) analyze the changes of thermal comfort in different seasons and land cover in Nanjing in China. Landsat images in four time points of 1994, 2000, 2010 and 2013 was used. The modified temperature-humidity index applied to explore the urban thermal comfort. The findings showed that the impacts of water bodies and built-up lands on thermal comfort were the most important in summer with being the most comfortable and uncomfortable types, respectively and the opposite results found in spring and winter. Additionally, the composition of the landscape was found a major factor affecting thermal comfort.

In most studies, the efficiency of satellite imagery has been proven useful for outdoor thermal comfort modeling. LST and vegetation cover index have been used to modeling of outdoor thermal comfort, while Taleghani (2018), Taleghani and Berardi (2018) and Yang et al. (2013) showed that other parameters, such as albedo, emissivity, and wetness can also affect the outdoor thermal comfort of a region.

Multiple linear regression model is one of common regression models in modeling outdoor thermal comfort. The least squares adjustment (LSA) can be used to determine the optimum values of the unknown coefficients in linear regressions. This method is based on minimization the sum of the squares error and applying it in linear or nonlinear mathematical models (Yan et al. 2018). LSA is high-performance, simple and user friendly (Schaffrin and Felus 2005). On the other hand, this model also can also be implemented with low number of training data (Ghilani 2017). While LSA can be useful, one of the most important assumptions of this model is multiple nonlinearity. That is, the predictive variables should not have a very high correlation with each other (Kumar et al. 2019, Cahyono et al. 2020). Different environmental and surface biophysical parameters were correlated with each other in a region. The use of these independent variables in regression models may lead to errors in modeling outdoor thermal comfort. Principle Component Analysis (PCA) can be very useful to solve the correlation challenge between predictive variables in the regression models for modeling outdoor thermal comfort. PCA is a numerical statistical method that converts a number of components dependent from multispectral image to a smaller number of uncorrelated linear combinations of variables in the name of the principal component (Zhang et al. 2014, Liu et al. 2017, Adami et al. 2018). In general, the first principal component (PC1) contains shared information of all bands used as input data in the PCA, i.e., spatial information, while the spectral specific information of each band falls into the other principal components (Wang et al. 2010, de Almeida et al. 2015, Firozjaei et al. 2019b);(de Almeida et al. 2015, Bansal et al. 2017, Liu et al. 2020).

The objective of this study is to propose a new approach for modeling outdoor thermal comfort using reflective and thermal infrared remote sensing data based on the PCA and LSA models. The unique contribution of this study to the literature is threefold: a) presentation of a LSA model for modeling outdoor thermal comfort using reflective and thermal infrared remote sensing data, which can take into account of key environmental parameters; b) The challenge of correlation among independent variables is solved by applying the PCs; and c) The presented LSA model shows the ability to model outdoor thermal comfort status in both absolute and relative terms.

2. Materials and methods

2.1. Study area

Tehran is a key center for production, housing, trade, distribution and transportation in Iran. It has a population of 8,895,947
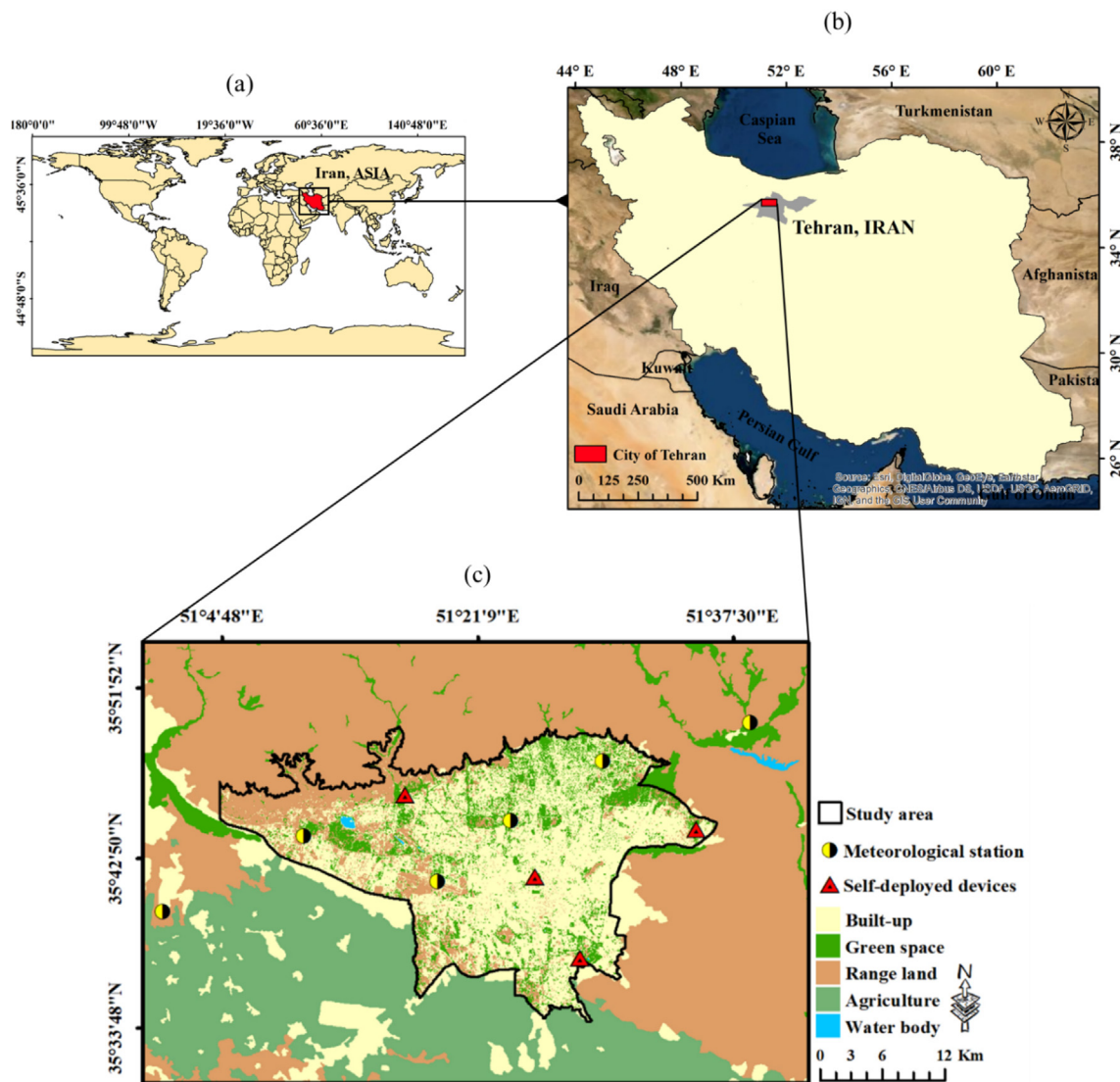
Fig. 1. Tehran and its suburb: (a) Iran location in world; (b) Geographical location of the Tehran in Iran; (c) Major land cover types around urbanized zone.

(worldpopulationreview 2018) that reaches exceeding 14 million people in daytime and stands as the 24th largest populated city in the world and the most populous city in western Asia. Ahmadnezhad et al. (2013) reported that 17 heat waves occurred in Tehran in 2001 to 2011, causing more than 1,069 mortality. In the summer of 2013, a heat wave sequence extended over three weeks with air temperature of more than 40 °C and broke the air temperature record in the last 60 years in Tehran. Also, the average annual frequency of heat waves during the period of 2005–2015 in Tehran metropolitan area was 43 heat waves per year, of which approximately on average, 50% of the waves occur during the warm season and 50% in the cold season (Keikhosravi 2019). The geographic location of the study area is shown in Fig. 1. Tehran is located where Dashte-e Kavir deserts touch Alborz mountains, hence, its climate can vary largely depending how each of the two landscapes play a dominant role. This means that its climate is largely heterogeneous so that the Northern districts have a dry cold climate, and the Southern parts have a dry warm climate. The height of this city ranges between 900 and 1800 m above sea level within 30 km. In the last 45-year season, Tehran has experienced its highest temperature at about 43 °C and its lowest temperature at about −15 °C. The average of relative humidity in Tehran is 40%, the dominant wind direction is west (270˚) and its average speed is 5.5 m/s. The mean annual rainfall varies from a maximum of 422 mm in the north to a

minimum of 145 mm in the south-east. The number of rainy days varies between 89 days in the north and 33 days in the south, while there are about 205 to 213 clear sky days. The land cover map and the area of each class for the case study are extracted based on the Landsat 8 image on 25 May 2018. According to Fig. 1, the area of built-up, green space, bare land and water body for the study area were 4800.61, 869.8, 13494.1 and 141.6 ha, respectively.

2.2. Data

This study used satellite imagery, meteorological, and land data sets to implement propose model for modeling outdoor thermal comfort. In this study a set of Landsat 8 satellite images (Path: 164, Row: 035), MODIS water vapor (MOD07) and LST (MOD11A1) products for the season of 2013–2018 were used. In this study, Landsat satellite imagery were used for modeling of surface biophysical parameters such as LST, albedo, land cover, brightness, greenness and wetness. The MOD07 and MOD11A1 products were used to calculate and accuracy assessment of LST obtained from Landsat images. Also, in this study, Advanced Spaceborne Thermal Emission and Reflection Radiometer (ASTER) Global Digital Elevation Model (GDEM) was used to modeling of incoming radiation and Temperature Lapse Rate (TLR) effect (Firozjaei et al. 2019a, Firozjaei et al. 2019c).
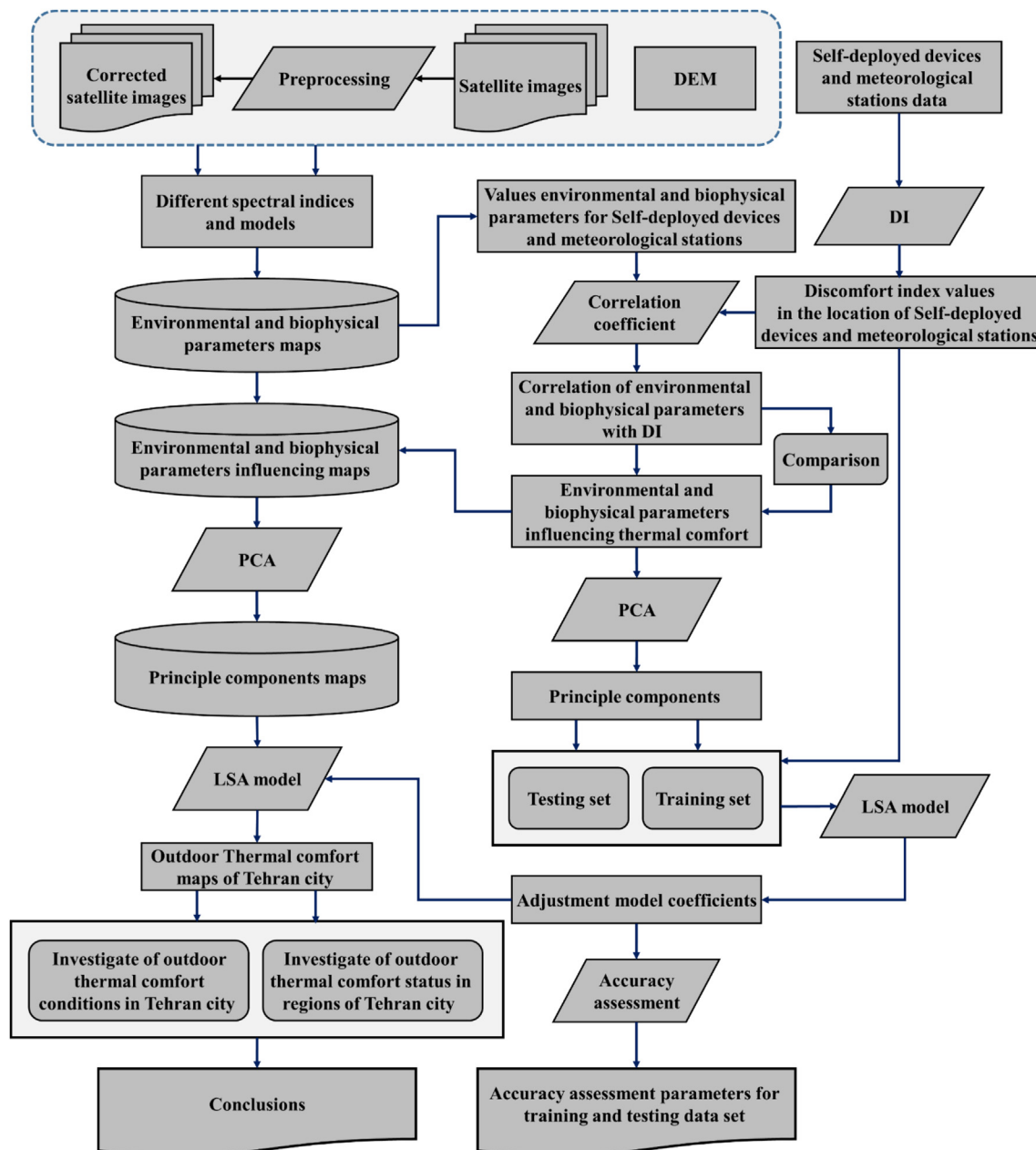
Fig. 2. The flowchart of the study.

Climatic data measured at six synoptic stations in the study area (Fig. 1), including air temperature, relative humidity, and soil temperature, were used. The recording time the climate data was simultaneous with the Landsat overpass during the 2013–2018. Meteorological and synoptic stations are located in the study area covering heterogeneous landscapes, so that the climatic conditions and heterogeneous topography of the case study are well covered. Additionally, ground data set was recorded by relative humidity and air temperature recording devices at the Landsat overpass was used. The Testo 184 G1 two-channel data logger was used for recording relative humidity and air temperature. Four of these devices were placed at a height of 2 m from the ground and continuously recorded relative humidity and air temperature for 37 days. The temperature recorder range by these devices is 20–70° C and relative humidity is 0–100%. The accuracy of recording relative humidity and air temperature by these devices was ± 0/5° C and ± 0.03%, respectively. In the present study, from relative humidity and air temperature data recorded by these devices

were used at the time of Landsat satellite passage on 12 July 2018, 28 July 2018 and 13 August 2018. From the training and testing dataset obtained field observation on 25 May 2018 were used in the classification process of land covers in the supervised classification algorithm. For each land type i.e., built-up, bare land, open space and water body, about 200 pixels and 150 pixels are chosen, respectively as a set of training and testing samples, for classification and accuracy assessment. To collect these samples, from a handheld GPS (error < 7 m) was used.

2.3. Methodology

The proposed conceptual model for modeling outdoor thermal comfort based on LSA is indicated in Fig. 2. In the first step, DI values for the location of synoptic stations were calculated based on the relative humidity and air temperature values. In the second step, different environmental and surface biophysical parameters maps, presented as supplementary data and the values of these parameters were extracted

4

Table 1
Environmental and surface biophysical parameters used in this study.

Parameters	Description	Reference
SULR	The Surface Upward Longwave Radiation (SULR) is the thermal radiation flux, which is emitted from the earth's surface to the atmosphere	(Allen et al. 2002, Firozjaei et al. 2018, Firozjaei et al. 2019c)
DSSR	The amount of Downward Surface Shortwave Radiation (DSSR) includes direct and diffuse solar radiation and direct and diffused reflected radiation from neighboring regions	
DSLR	The Downward Surface Longwave Radiation (DSLR) is the downward thermal radiation flux from the atmosphere.	
NDVI	The Normalized Difference Vegetation Index (NDVI) indicates vegetation cover information.	(Tucker 1979)
NDBI	The Normalized Difference Built-up Index (NDBI) indicates Brightness information, including the percentage of impervious surface, including bare land and built-up lands	(Zha et al. 2003)
NDWI	The Normalized Difference Water Index (NDWI) indicating moisture information including water-related complications, soil moisture, Plant and built-up lands	(Gao 1996)
Albedo	The albedo is the proportion of reflected solar radiation to the total solar radiation emitted to land surface. The value of this parameter depends on the type, sex, and amount of solar radiation absorbed by the phenomena.	(Taleghani 2018)
SAVI	Soil-Adjusted Vegetation Index (SAVI) is a transformation technique that minimizes soil brightness influences from spectral vegetation indices involving red and Near-Infrared (NIR) wavelengths.	(Huete 1988)
Brightness	First components of Tasseled Cap Transformation (TCT)	(Liu et al. 2014, Liu et al. 2015)
Greenness	Second components of Tasseled Cap Transformation (TCT)	
Wetness	Third components of Tasseled Cap Transformation (TCT)	

Table 2
Outdoor thermal comfort categories depending on the DI values.

Outdoor thermal comfort categories	DI values (°C)
Hyper glacial	<-40
Glacial	−39.9 to −20
Extremely cold	−19.9 to −10
Very cold	−9.9 to −1.8
Cold	−1.7 to 12.9
Cool	13−14.9
Comfortable	15−19.9
Hot	20−26.4
Very hot	26.5−29.9
Torrid	>30

at the location of the synoptic stations. In the third step, based on the correlation coefficient between DI index values and the environmental and surface biophysical parameters of different values, environmental and surface biophysical parameters influencing outdoor thermal comfort were identified. In the fourth step, based on the PCA, the first and second PCs of the environmental and surface biophysical parameters influencing outdoor thermal comfort were calculated. Then, the LSA model was employed to estimation of impact of first and second PCs on outdoor thermal comfort. Finally, based on the optimal coefficients calculated separately for the first and second PCs and maps of the first and second PCs, outdoor thermal comfort maps were produced and the outdoor thermal comfort conditions in Tehran were investigated.

2.3.1. Preprocessing and environmental and surface biophysical parameters modeling

In this study, atmosphere correction was conducted using the Fast Line-of-sight Atmospheric Analysis of Hypercubes (FLAASH) algorithm (Cooley et al. 2002, Weng et al. 2019). The downloaded Landsat imagery from the USGS are considered suitable for time-series analysis. The geo-registration was consistent and an Root Mean Square Error (RMSE) of < 12 m was achieved (Moghaddam et al. 2018, Weng et al. 2019). The geometric correction of image-to-image was conducted to match the Landsat 8 image and GDEM.

The outdoor thermal comfort in the urban environment is influenced by the interactions between the climatic conditions and the structural characteristics of urban areas (Potchter and Ben-Shalom 2013). Our literature review reveals that the heterogeneity in the urban surfaces characteristics causes outdoor thermal comfort heterogeneity for citizens in different urban regions, which are mainly affected by environmental and surface biophysical parameters, including DSSR, DSLR, SULR, brightness, greenness, and wetness of the surface (Wang et al. 2004, Zhang et al. 2009, Van Hove et al. 2015, Qaid et al. 2016).

The environmental and biophysical parameters modeled in this study are shown in Table 1.

2.3.2. Outdoor thermal comfort in the locations of self-deployed devices and meteorological stations

In this study, using air temperature and relative humidity values recorded at self-deployed devices and meteorological stations, based on the equation (1), outdoor thermal comfort is calculated for the location of each synoptic station at the Landsat overpass.

$$DI = T - 0.55(1 - 0.01RH)(T - 14.5) \tag{1}$$

Where DI is the outdoor thermal comfort indicator, T air temperature (° C) and RH relative humidity (%) in the location of the self-deployed devices and synoptic stations. The DI index was introduced by Thom (1959), which calculation the human thermal comfort in open spaces based on the relative humidity and air temperature. The constant coefficients in this model are calculated based on the communication between air temperature and relative humidity variables with modeled thermal comfort based on the metabolic information of the human body (Thom 1959).

In several studies, the efficiency of DI has been proven for modeling the outdoor thermal comfort situation in vast regions (Wang et al. 2004, Toy et al. 2007, Sobrino et al. 2013, Coccolo et al. 2016, Xu et al. 2017, Mushore et al. 2018). The results of DI can be categorized according to Table 2.

After calculating DI values for different dates from 2013 to 2018, the environmental and surface biophysical parameters were extracted for the geographic location of self-deployed devices and meteorological stations. To determine the environmental and surface biophysical parameters influencing outdoor thermal comfort, the correlation coefficient between each of these parameters with the DI values in the geographic locations of self-deployed devices and meteorology was calculated. The parameters that have a higher correlation coefficient with outdoor thermal comfort index were used in the modeling. For each group of surface biophysical characteristics, including brightness, greenness and wetness, the parameter that has a higher correlation coefficient with outdoor thermal comfort index was selected.

2.3.3. Proposed model based on LSA for modeling outdoor thermal comfort

Since there is a strong correlation among independent variables, e.g., environmental and surface biophysical parameters, their application in the LSA model is problematic due to data redundancy. To solve this problem, PCA was used in order to minimize the correlation (González-Audícana et al. 2004, Jolliffe 2011, Ha et al. 2013). Because the scale and unit of environmental parameters used are different, the PCA-based correlation matrix has been used in this study (Croux and
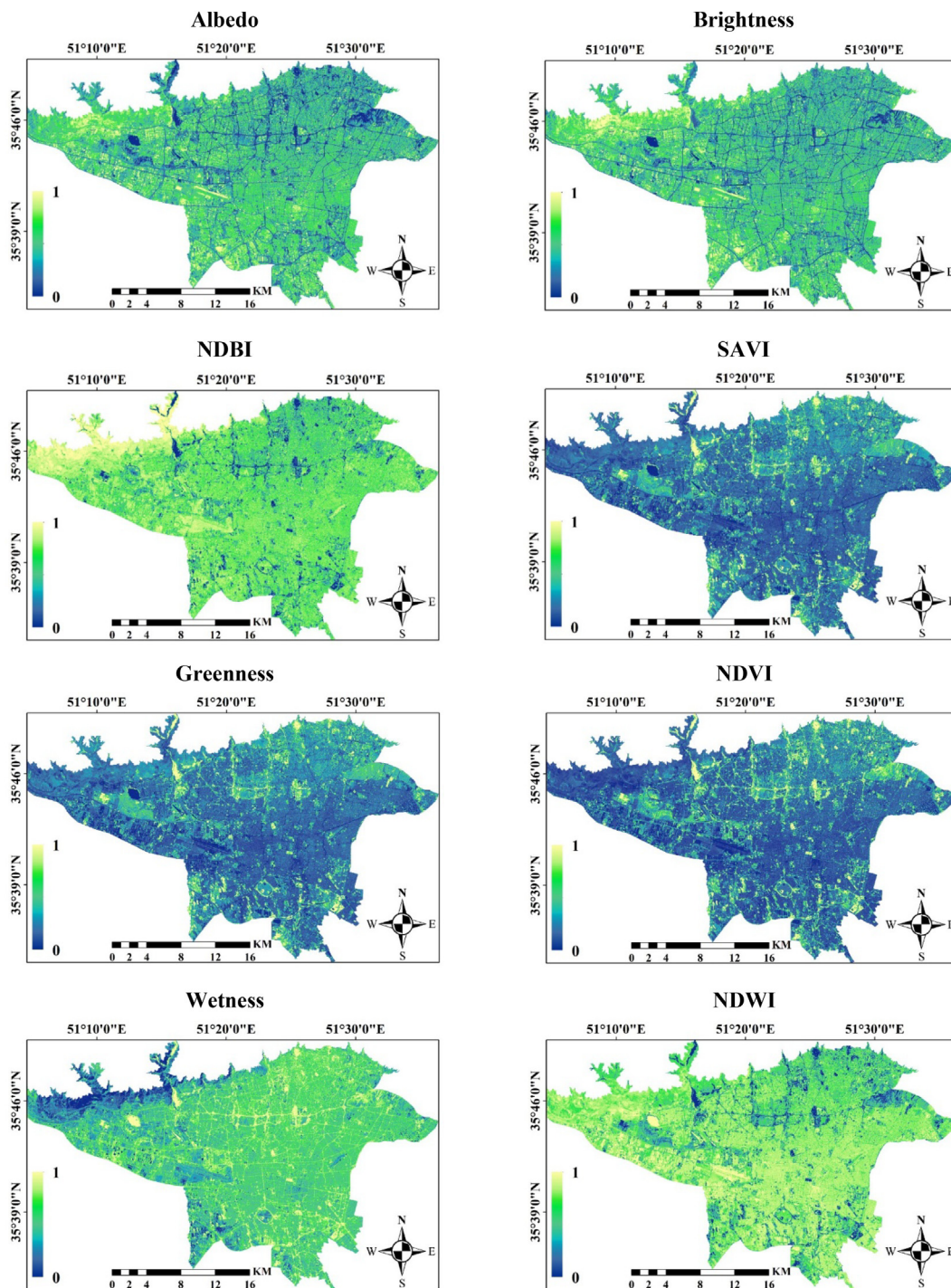
Fig. 3. Environmental and surface biophysical parameters maps for 13 August 2018.

Haesbroeck 2000, Borgognone et al. 2001).

In this study, PCs of environmental and surface biophysical parameters influencing DI values in the locations of self-deployed devices and meteorological stations, were used with equation (2).

$$DI_{Model} = a_0 + a_1 PC1 + a_2 PC2 \qquad (2)$$

In equation (2), PC1 and PC2 represent the first and second PCs of the environmental and surface biophysical parameters influencing outdoor thermal comfort, and a_0, a_1 and a_2 are coefficients. In order to calculate the optimal values of the coefficients while minimizing the remaining values of variance, i.e., minimizing the RMSE between the modeled outdoor thermal comfort and the actual outdoor thermal

comfort, all coefficients were calculated (Fan 1997, Wolf and Ghilani 1997). In this case, for each observation, an equation is casted and using the LSA method, the optimal values of the regression coefficients will be calculated. Equations (3), (4) and (5) show the LSA form.

$$B = DI = A. X \rightarrow (B - A. X) \rightarrow min = LeastSquareAdjustment \qquad (3)$$

$$A = \begin{bmatrix} 1 & PC1_1 & PC2_1 \\ .. & \cdots\cdots. & \cdots\cdots\cdots. \\ 1 & PC1_n & PC2_n \end{bmatrix} \qquad (4)$$

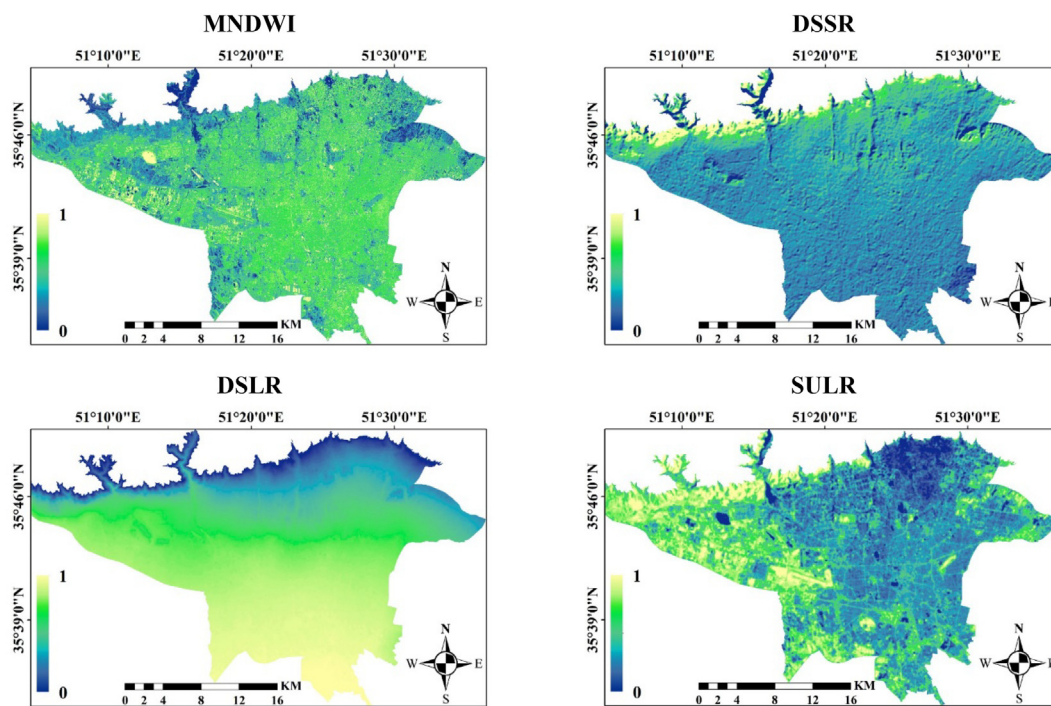$$X = [a_0 \quad a_1 \quad a_2]^t \qquad (5)$$

Fig. 3. (*continued*)

Table 3
Correlation coefficient among the environmental and surface biophysical parameters influencing outdoor thermal comfort.

Parameters	DSSR	DSLR	SULR	Brightness	Greenness	Wetness
DSSR	1	0.15	0.74	0.18	0.21	0.05
DSLR	–	1	0.14	0.08	0.13	0.09
SULR	–	–	1	0.31	0.28	0.21
Brightness	–	–	–	1	0.50	0.05
Greenness	–	–	–	–	1	0.18
Wetness	–	–	–	–	–	1

Table 4
Variance and correlation coefficient of PCs of environmental and surface biophysical parameters influencing outdoor thermal comfort.

Components	PC1	PC2	PC3	PC4	PC5	PC6
Variance	4579	123	2	0.02	0.006	0.0008
R^2	0.81	0.05	0.003	0.006	0.0009	0.0002
Eigenvalue	8.45	1.12	0.18	0.10	0.02	0.01

By calculating optimal coefficients values and placing in equation (2), DI thermal index maps for the case study were obtained.

In this study, the geographical location of the meteorological stations during the period 2013–2016 were used as training data for calculating the unknown coefficients of the LSA model. Furthermore, the geographic location of self-deployed devices and meteorological stations data synchronized with the images for the season 2017 to 2018 as testing set were used to assess the accuracy of the model. To do so, the correlation coefficients and RMSE were computed between modeled DI and DI obtained from self-deployed devices and weather stations. Then, the outdoor thermal comfort condition of Tehran for annual warm and cold seasons across different urban districts and land types in 2017 and 2018 was analyzed. For a meaningful evaluation results based on general population, the correlation coefficients between the modeled DI and the number of hospital emergency visits due to heat stroke at 2017 and 2018 summer in urban districts was calculated. To prepare the urban land cover map, From the Landsat 8 satellite image on 25 May

2018 and the Maximum Likelihood Classification (MLC) algorithm was used (Otukei and Blaschke 2010).

3. Results and discussion

Environmental and surface biophysical parameters were modeled for different timestamps. LST was calculated for different time-steps using the Split-Window (SW) (Jiménez-Muñoz et al. 2014) and the Single-Channel (SC) (Jiménez-Muñoz et al. 2014, Yu et al. 2014) algorithms. The RMSE and correlation coefficient between the LST derived Landsat imagery and soil temperature recorded in the location of the synoptic stations for the SW algorithm were 0.74 and 3.2, respectively, and for the SC algorithms 0.77 and 2.8, respectively. Also, the difference between the mean LST obtained from the SW and SC algorithms with the average of MOD11A1 product were 2.2 and 1.8, respectively. Accordingly, the LST calculated from the SC algorithm was used for modeling SULR. The spatial distribution of the environmental and surface biophysical parameters of the case study are heterogeneous (Fig. 3).

The correlation coefficient between value of DI and each environmental and surface biophysical parameters including brightness, wetness, greenness, NDBI, NDWI, albedo, DEM, FVC, NDVI, SULR, DSLR, and DSSR in geographic location of self-deployed devices and meteorological stations are 0.38, 0.30, 0.28, 0.01, 0.02, 0.30, 0.02, 0.01, 0.01, 0.85, 0.21, and 0.02, respectively. The DSSR, DSLR, and SULR, and the surface biophysical parameters of brightness, greenness and wetness had the highest effect on the DI values. This set of environmental and surface biophysical parameters was used for the first time in modeling outdoor thermal comfort.

Previous studies have shown that environmental and surface biophysical parameters, such as LST, incoming and upwelling radiation, built-up lands, vegetation cover, and albedo, brought an impact on the temporal and spatial changes of the measured outdoor thermal comfort indicators at synoptic stations. In this study, by replacing SULR with LST, the influence of emissivity parameter is also considered in the modeling outdoor thermal comfort for the first time. As brightness increases, the sensible heat flux increases. This result suggests that increased surface brightness can significantly affect the outdoor thermal
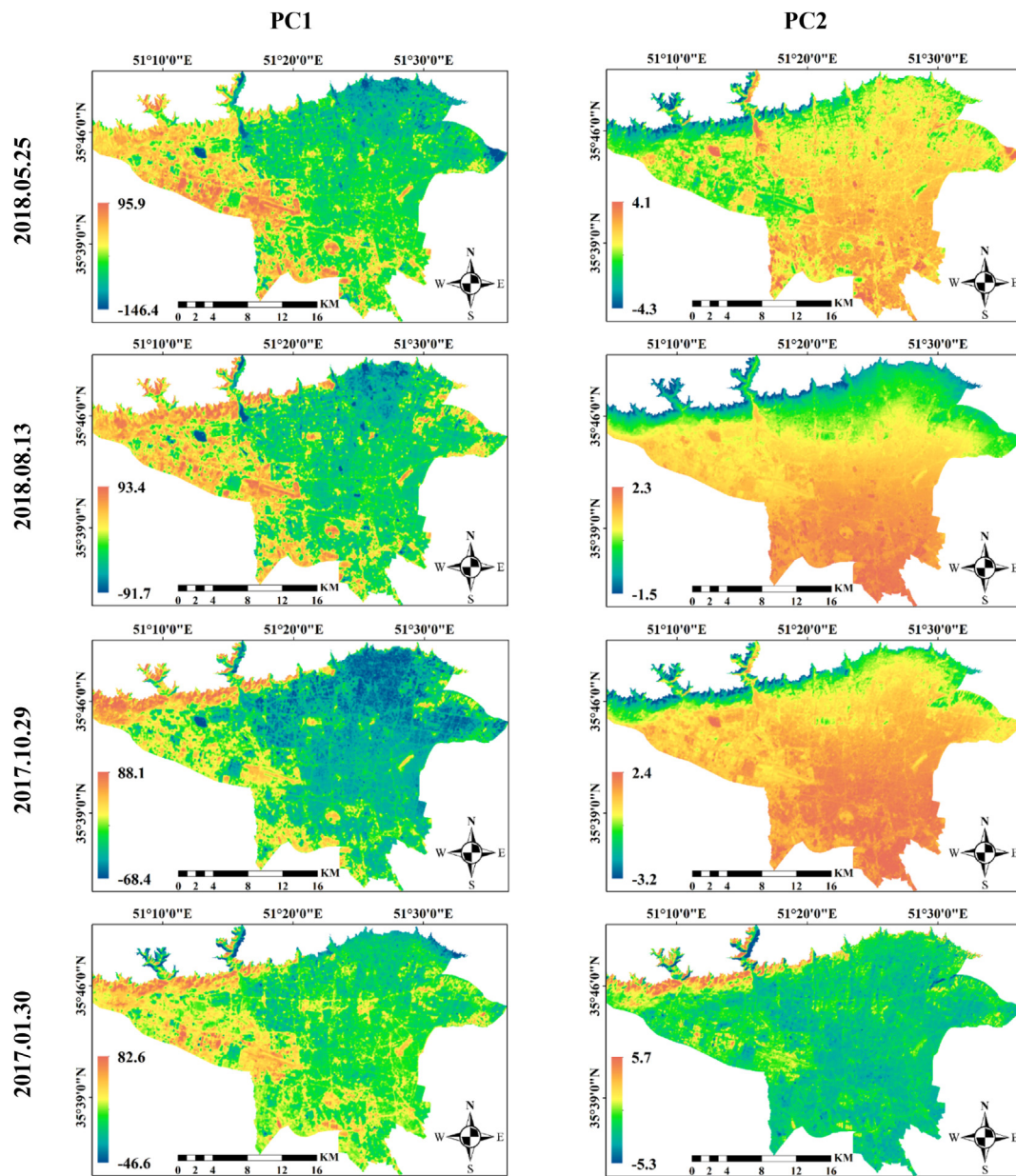
PC1   **PC2**

Fig. 4. A sample of the first and second components maps for spring, summer, autumn and winter in 2017 and 2018.

comfort in urban open spaces. Although it increases surface albedo of asphalt as a factor in reducing LST, a few studies such as (Taleghani 2018) considered the outdoor thermal comfort of the pedestrian. The outdoor thermal comfort mainly depends on the mean radiant temperature, while the increase in albedo increases the short-wave solar radiation from the surface to the atmosphere. Although pedestrians use the high albedo surface to reduce the surface of the asphalt, they suffer from an increase in the reflected short-wave radiation from surface.

In nature, many of the environmental and surface biophysical parameters are highly correlated (Table 3). Meanwhile, the correlation coefficient between the DSSR and SULR and between the Brightness and Greenness were 0.74 and 0.50, respectively. In Zoo et al. (2017), environmental and surface biophysical parameters were used directly for modeling outdoor thermal comfort in a multivariate regression model (Xu et al. 2017). Given the correlation between these parameters, their direct application in the LSA model is statistically challenged. This challenge is addressed for the first time in this study.

To overcome the challenge of correlation between independent variables, PCA was used for the first time in modeling outdoor thermal

comfort. The majority of non-redundant information related to environmental and surface biophysical parameters were embedded in the first and second PCs. The correlation coefficient between the first and second PCs with the DI values in the location of the synoptic station is 0.81 and 0.05, respectively (Table 4). The eigenvalues of the first and second component is 8.45 and 1.12, respectively, which is much higher than the eigenvalues of the other components. These results show that PC1 and PC2 contained a very high percentage of primary environmental and biophysical parameters information. The value of correlation between PC1 and PC2 information is negligible and close to zero. For this reason, outdoor thermal comfort was modeled based on LSA, the first and second PCs for the first time.

Based on equation (2), the RMSE and correlation coefficient between the modeled and observed outdoor thermal comfort values at the synoptic station for the training data set (from the beginning of 2013 to the end of 2016) were 1.80 °C and 0.86, respectively and for the testing data set (2017 and 2018) are 0.89 and 2.04, respectively. Also, the RMSE and correlation coefficient between the modeled and observed outdoor thermal comfort at 4 self-deployed devices for 12 July 2018, 28
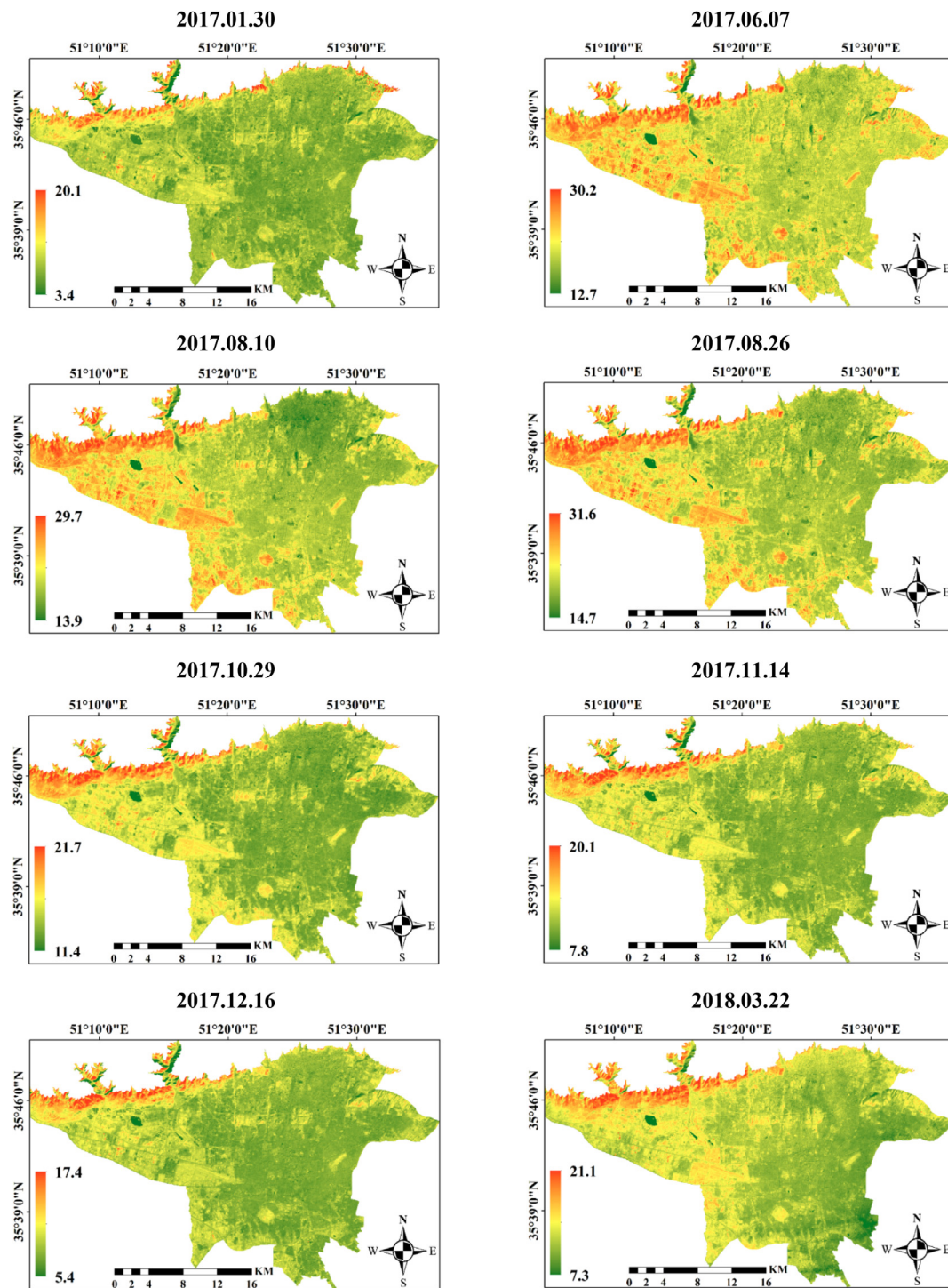
Fig. 5. DI maps in Tehran, Iran, in 2017 and 2018.

July 2018 and 13 August 2018 were investigated and the results are 1.15 °C and 0.85, respectively. The results indicant the capability of the proposed model for the modeling outdoor thermal comfort. The spatial and temporal distribution of the first and second principal components for spring, summer, autumn and winter in case study is variable (Fig. 4).

Based on equation (11), in general, the western and northwestern districts of the case study had the highest DI values and the central, north and south-east districts the lowest DI values (Fig. 5).

The mean DI varied over different seasons. The highest and lowest DI values were discovered on 28 July 2018 and 30 January 2017, respectively (Fig. 6). The trend of changes in mean DI and PC1 on different dates is similar together.

Generally, the average value of the DI indicates that these dates can be classified into two groups, the warm and cold seasons. On 30 January 2017, 29 October 2017, 14 November 2017, 16 December 2017 and 22 March 2018 with the average of the DI, 12.6 °C belonged to the cold season category, and the other of the dates to the mean DI are 12.6 °C in the warm category.

For the cold season, the area and the number of clusters with high DI values was found lower than the warm season of year (Fig. 7). The average of the DI in the warm season of year yielded 8.5 °C higher than the cold season of the year. The high value of the DI did not indicate
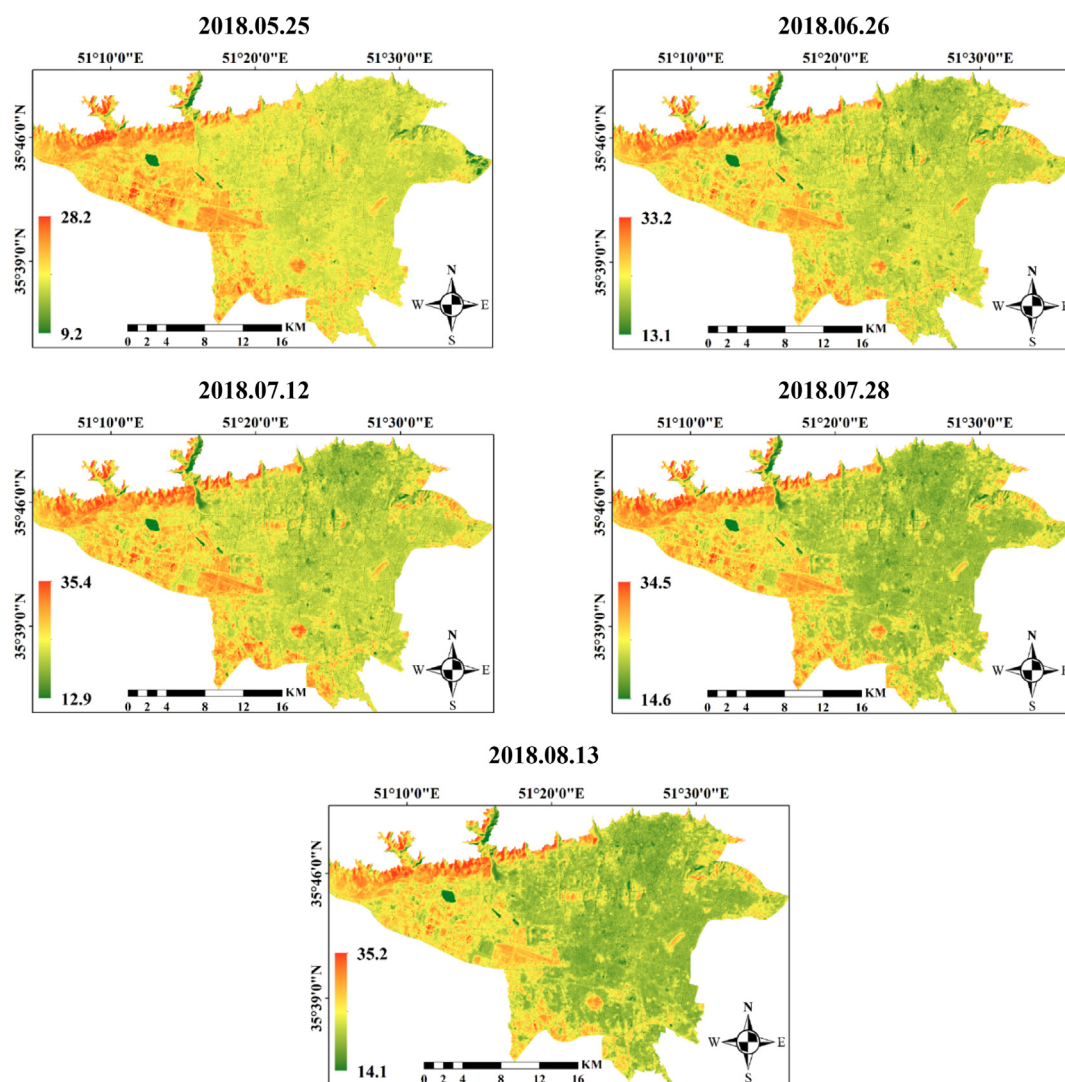
2018.05.25

2018.06.26

2018.07.12

2018.07.28

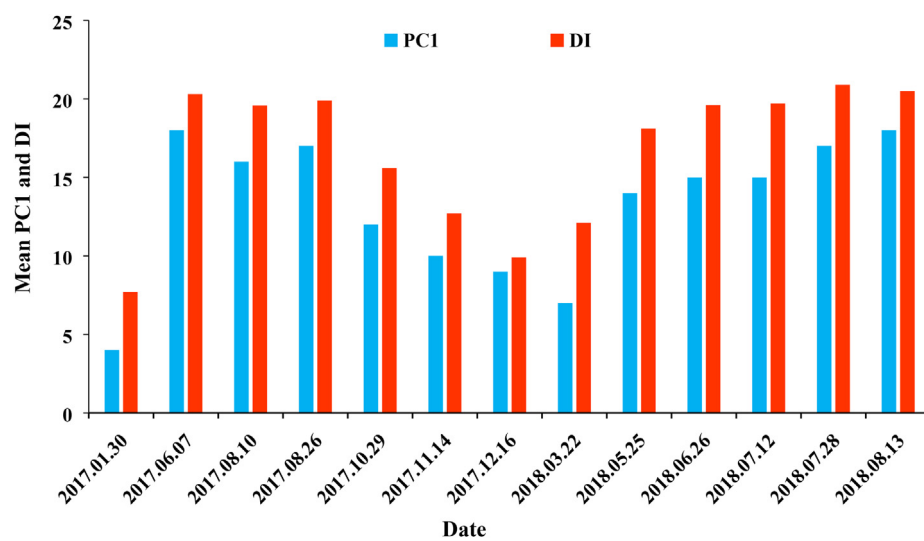### 2018.08.13

Fig. 5. (*continued*)

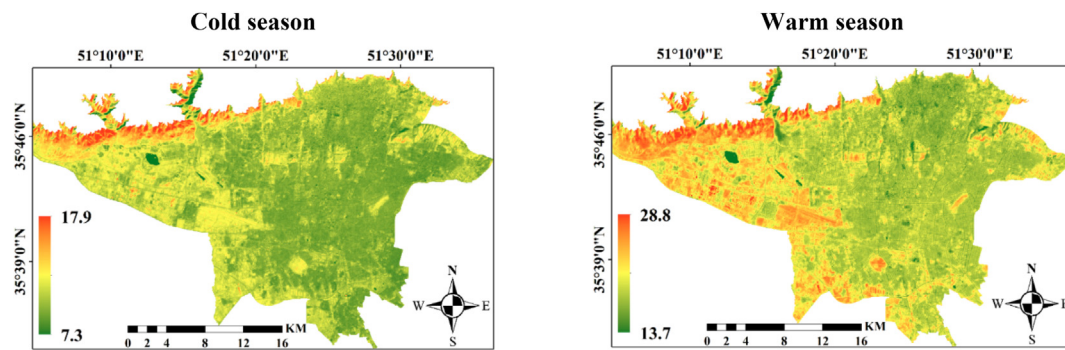**Fig. 6.** The mean PC1 and DI for different timestamps.

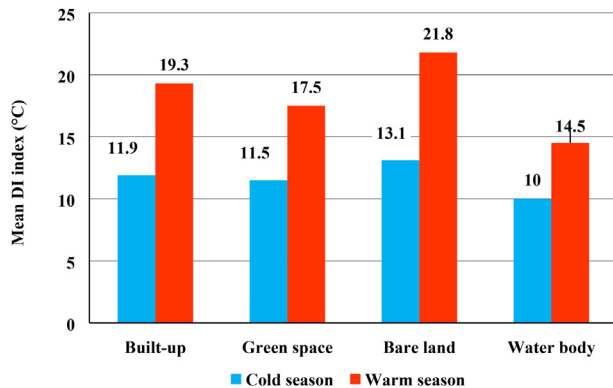**Fig. 7.** The mean DI maps for warm and cold seasons of years.

Fig. 8. The mean DI for each land cover in the warm and cold seasons of the year.

favorable conditions for outdoor thermal comfort. Analysis of this indicator for the warm and cold season of year can be different, and vice versa. In the warm season of year, the low DI value was favorable, but in the cold season of year, the high value of this index was favorable for outdoor thermal comfort.

Considering the effect of land cover on environmental and surface biophysical parameters, it can be concluded that DI outdoor thermal comfort values in different land cover was different. In both warm and cold seasons of year the average of the DI for bare land and water body was higher and lower than other land covers (Fig. 8). Earlier studies by (Xu et al. 2017, Mushore et al. 2018, Song and Wu 2018) have shown that green space and water bodies improved the outdoor thermal comfort in a region. The results indicate that the difference between the mean DI value of the land covers in the warm season of year was higher than the cold season of the year.

For a more accurate examination of the outdoor thermal comfort conditions, the mean DI for different urban districts were calculated. The results show that in both warm and cold season of years, the

districts of 22, 21, 9, 18, 19 and 5, which are located in the geographical directions of the west, northwest, and south-west, possessed higher outdoor thermal comfort values than others. In the warm season of the year, areas 1, 3, 6, 8, 11 and 10, and in the cold season of the year, districts 8, 14, 12, 11, 10, 15 and 17, detected low DI values (Fig. 9).

It should be noted that high or low DI values for a specific spot in the study area at a particular time did not necessarily indicate the presence or absence of a favorable outdoor thermal comfort. Previous studies (Toy et al. 2007, Sobrino et al. 2013, Coccolo et al. 2016) indicated that according to human body's metabolism, a DI value between 15 °C and 19.9 °C perceived as the most favorable condition. The correlation coefficients between the modeled DI and the number of hospital emergency visits due to heat stroke at warm season in urban districts was 0.89. The results indicate the significance of the results based on general population. According to Table 2, the results of DI scores can be classified to cold, cool, comfortable, hot, very hot and torrid zones (Fig. 10).

During the cold seasons of the year, the city of Tehran consisted of cold, cool and comfortable categories. But, for the warm season of the year, the area contained cool, comfortable and hot categories. In the warm season, the cold category included water bodies. In the cold season, the comfortable category was discovered in the west and northwest of the studied area, while the central, north and south-east districts were mostly in the cold and cool categories. However, in the warm season, the central, northern, northeastern and southeastern districts of the comfort category were located in the comfort zone, and the western, northwest, and southwestern districts on the warm category, indicating the condition of outdoor thermal comfort was unsuitable for these Districts. In the northern part of Tehran, the climate is temperate and mountainous, and semi-arid in some places. The precipitation is usually high in winter. In March, the weather temperature is increasing and the weather is warming up in late April. In early June, the weather is relatively warm. The climate of Tehran is warm and dry in desert and southern areas, while it is cold and semi-humid in highlands, cold with long winters. The hottest months of the year are
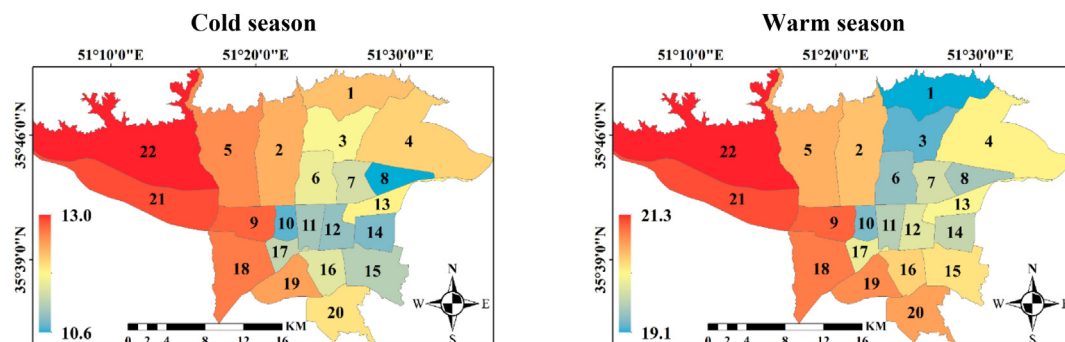

Fig. 9. The mean DI values for different urban districts in warm and cold seasons of the year in Tehran, Iran.
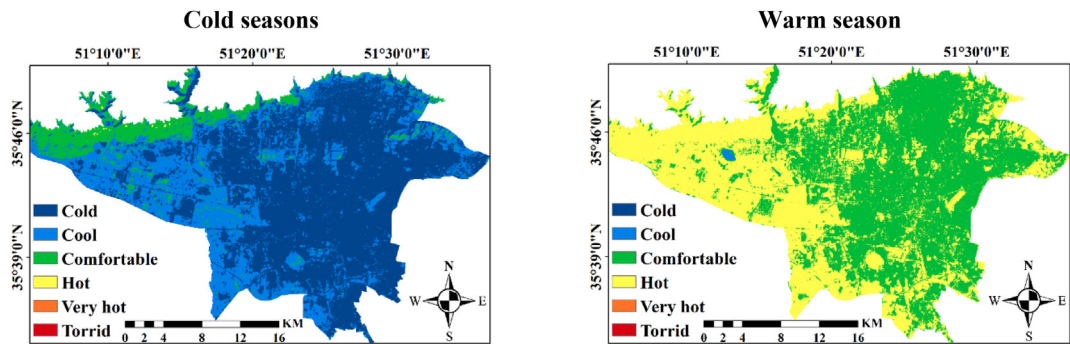
Fig. 10. The classified DI zones for the warm and cold seasons of the year in Tehran, Iran.

Table 5
The percentage of area each of category in the case study for the warm and cold seasons of the year.

Outdoor thermal comfort categories	warm season	Cold season
Cold	0.00	58.13
Cool	0.16	31.81
Comfortable	52.74	10.04
Hot	47.09	0.00
Very hot	0.00	0.00
Torrid	0.00	0.00

reported in August and September with an average temperature of 35 to 45 °C, and the coldest months of the year, January and February, with a temperature of −5 °C. The northern part of Tehran and Shemiranat are also moderate in the summer. In the warm season of the year, 52% of the area of the study was classified as a comfortable category and 47% was made up of warm category. For the cold season, cold, cool, and comfortable categories covered 58%, 31%, and 10% of the area, respectively (Table 5).

4. Conclusions

In this study, we have demonstrated that a LSA based model can be developed to model outdoor thermal comfort conditions with remotely sensed and climate datasets. The novelty of this study is threefold: a) presentation of a LSA model for modeling outdoor thermal comfort using reflective and thermal infrared remote sensing data; b) The challenge of correlation among independent variables is solved by applying PCA; and c) The presented LSA model shows the ability to model outdoor thermal comfort status in both absolute and relative terms. By replacing SULR with LST, the influence of the emissivity parameter was also considered in the modeling for the first time. Due to the correlation between the environmental and surface biophysical parameters, their direct application in the LSA model is statistically challenged. This challenge is addressed for the first time in this study. The result of the case study in Tehran, Iran shows that the mean DI value in the warm season was higher than that in the cold season. In both warm and cold seasons, the average values of DI for bare land yielded higher than other land covers, but those of water bodies always lower than others. The difference between the mean DI value of the land covers in the warm season of year was higher than that of the cold season. Our findings indicate that cold, cool and comfortable categories of outdoor thermal comfort appeared in the cold season, while cool, comfortable and hot categories in the warm season. The proposed LSA model has the capability of modeling outdoor thermal comfort in absolute and relative terms. The correlation coefficient and RMSE between the modeled and observed outdoor thermal comfort values at the locations of self-deployed devices and meteorological stations for the training and testing data sets proved the efficiency of the proposed model. However, the coefficients must be adjusted for each case study in the modeling, so

that better communication of its outcome would be possible with local policy makers and the general public of a city. In arid regions or regions with hot summers, our approach can help to identify extreme and intolerable areas for certain demographic and socioeconomic groups. In future studies, it is suggested to explore the feasibility of modeling nighttime outdoor thermal comfort because urban heat island effect can be more apparent in the evening. Furthermore, satellite images at finer resolution along with land cover data reflecting fine landscape variations can yield more accurate maps of outdoor thermal comfort.

CRediT authorship contribution statement

Naeim Mijani: Conceptualization, Data curation, Methodology. **Seyed Kazem Alavipanah:** Supervision. **Mohammad Karimi Firozjaei:** Methodology, Writing - original draft. **Jamal Jokar Arsanjani:** Investigation, Writing - review & editing. **Saeid Hamzeh:** Supervision. **Qihao Weng:** Writing - review & editing, Supervision.

Declaration of Competing Interest

The authors declare that they have no known competing financial interests or personal relationships that could have appeared to influence the work reported in this paper.

Appendix A. Supplementary data

Supplementary data to this article can be found online at https://doi.org/10.1016/j.ecolind.2020.106555.

References

Adami, M., Bernardes, S., Arai, E., Freitas, R.M., Shimabukuro, Y.E., Espírito-Santo, F.D., Rudorff, B.F., Anderson, L.O., 2018. Seasonality of vegetation types of South America depicted by moderate resolution imaging spectroradiometer (MODIS) time series. Int. J. Appl. Earth Obs. Geoinf. 69, 148–163.
Ahmadnezhad, E., Holakouie Naieni, K., Ardalan, A., Mahmoodi, M., Yunesian, M., Naddafi, K., Mesdaghinia, A.R., 2013. Excess mortality during heat waves, Tehran Iran: an ecological time-series study. Journal of research in health sciences 13, 24–31.
Allen, R., Tasumi, M., Trezza, R., Waters, R., Bastiaanssen, W., 2002. SEBAL (Surface Energy Balance Algorithms for Land). Advance Training and Users Manual-Idaho Implementation, version 1, 97.
Arghavani, S., Malakooti, H., Bidokhti, A.-A.A.A., 2020. Numerical assessment of the urban green space scenarios on urban heat island and thermal comfort level in Tehran Metropolis. Journal of cleaner production:121183.
Bansal, S., Katyal, D., Garg, J., 2017. A novel strategy for wetland area extraction using multispectral MODIS data. Remote Sens. Environ. 200, 183–205.
Borgognone, M., a. G., J. Bussi, and G. Hough., 2001. Principal component analysis in sensory analysis: covariance or correlation matrix? Food Qual. Prefer. 12, 323–326.
Brunsell, N., 2006. Characterization of land-surface precipitation feedback regimes with remote sensing. Remote Sens. Environ. 100, 200–211.
Cahyono, B.K., Aditya, T., Istarno, I., 2020. The Least Square Adjustment for Estimating the Tropical Peat Depth Using LiDAR Data. Remote Sensing 12, 875.
Y. Cai Y. Chen C. Tong Spatiotemporal evolution of urban green space and its impact on the urban thermal environment based on remote sensing data: A case study of Fuzhou City 2019 Urban Forestry & Urban Greening China.
Choi, J.-H., Yeom, D., 2019. Development of the data-driven thermal satisfaction

prediction model as a function of human physiological responses in a built environment. Build. Environ. 150, 206–218.

Coccolo, S., Kämpf, J., Scartezzini, J.-L., Pearlmutter, D., 2016. Outdoor human comfort and thermal stress: A comprehensive review on models and standards. Urban Clim. 18, 33–57.

Cooley, T., G. Anderson, G. Felde, M. Hoke, A. Ratkowski, J. Chetwynd, J. Gardner, S. Adler-Golden, M. Matthew, and A. Berk. 2002. FLAASH, a MODTRAN4-based atmospheric correction algorithm, its application and validation. Pages 1414-1418 in Geoscience and Remote Sensing Symposium, 2002. IGARSS'02. 2002 IEEE International. IEEE.

Croux, C., Haesbroeck, G., 2000. Principal component analysis based on robust estimators of the covariance or correlation matrix: influence functions and efficiencies. Biometrika 87, 603–618.

de Almeida, T.I.R., Penatti, N.C., Ferreira, L.G., Arantes, A.E., C. H. do Amaral., 2015. Principal component analysis applied to a time series of MODIS images: the spatio-temporal variability of the Pantanal wetland, Brazil. Wetlands Ecol. Manage. 23, 737–748.

Fan, H. 1997. Theory of errors and least squares adjustment. Tekniska högskolan.

Feng, L., Zhao, M., Zhou, Y., Zhu, L., Tian, H., 2020. The seasonal and annual impacts of landscape patterns on the urban thermal comfort using Landsat. Ecol. Ind. 110, 105798.

Firozjaei, M., Fathololuomi, S., Alavipanah, S., Kiavarz, M., Vaezi, A., Biswas, A., Ghorbani, A., 2019a. Modeling the impact of surface charactristics on the near surface temperature lapse rate. The International Archives of Photogrammetry, Remote Sensing and Spatial Information Sciences 42, 395–399.

Firozjaei, M.K., Alavipanah, S.K., Liu, H., Sedighi, A., Mijani, N., Kiavarz, M., Weng, Q., 2019b. A PCA–OLS Model for Assessing the Impact of Surface Biophysical Parameters on Land Surface Temperature Variations. Remote Sensing 11, 2094.

Firozjaei, M.K., Fathololoumi, S., Kiavarz, M., Arsanjani, J.J., Alavipanah, S.K., 2020a. Modelling surface heat island intensity according to differences of biophysical characteristics: A case study of Amol city. Iran. Ecological Indicators 109, 105816.

M.K. Firozjaei M. Kiavarz O. Nematollahi M. Karimpour Reihan S.K. Alavipanah An evaluation of energy balance parameters, and the relations between topographical and biophysical characteristics using the mountainous surface energy balance algorithm for land (SEBAL). International Journal of Remote Sensing:1–31 2019.

Firozjaei, M.K., Nematollahi, O., Mijani, N., Shorabeh, S.N., Firozjaei, H.K., Toomanian, A., 2018. An integrated GIS-based Ordered Weighted Averaging Analysis for Solar Energy Evaluation in Iran: Current Conditions and Future Planning. Renewable Energy.

Firozjaei, M.K., Sedighi, A., Argany, M., Jelokhani-Niaraki, M., Arsanjani, J.J., 2019d. A geographical direction-based approach for capturing the local variation of urban expansion in the application of CA-Markov model. Cities 93, 120–135.

Firozjaei, M.K., Weng, Q., Zhao, C., Kiavarz, M., Lu, L., Alavipanah, S.K., 2020b. Surface anthropogenic heat islands in six megacities: An assessment based on a triple-source surface energy balance model. Remote Sens. Environ. 242, 111751.

Gao, B.-C., 1996. NDWI—A normalized difference water index for remote sensing of vegetation liquid water from space. Remote Sens. Environ. 58, 257–266.

Ghilani, C.D., 2017. Adjustment computations: spatial data analysis. John Wiley & Sons.

González-Audícana, M., Saleta, J.L., Catalán, R.G., García, R., 2004. Fusion of multispectral and panchromatic images using improved IHS and PCA mergers based on wavelet decomposition. IEEE Trans. Geosci. Remote Sens. 42, 1291–1299.

Ha, W., Gowda, P.H., Howell, T.A., 2013. A review of potential image fusion methods for remote sensing-based irrigation management: part II. Irrig. Sci. 31, 851–869.

Hami, A., Abdi, B., Zarehaghi, D., Maulan, S.B., 2019. Assessing the thermal comfort effects of green spaces: A systematic review of methods, parameters, and plants' attributes. Sustainable cities and society:101634.

Huete, A.R., 1988. A soil-adjusted vegetation index (SAVI). Remote Sens. Environ. 25, 295–309.

Jiménez-Muñoz, J.C., Sobrino, J.A., Skoković, D., Mattar, C., Cristóbal, J., 2014. Land surface temperature retrieval methods from Landsat-8 thermal infrared sensor data. IEEE Geosci. Remote Sens. Lett. 11, 1840–1843.

Ian Jolliffe Principal Component Analysis Miodrag Lovric International Encyclopedia of Statistical Science 2011 Springer Berlin Heidelberg Berlin, Heidelberg 1094 1096 10.1007/978-3-642-04898-2_455 http://link.springer.com/10.1007/978-3-642-04898-2_455.

Katavoutas, G., Assimakopoulos, M.N., Asimakopoulos, D.N., 2016. On the determination of the thermal comfort conditions of a metropolitan city underground railway. Sci. Total Environ. 566, 877–887.

Keikhosravi, Q., 2019. The effect of heat waves on the intensification of the heat island of Iran's metropolises (Tehran, Mashhad, Tabriz, Ahvaz). Urban Clim. 28, 100453.

Kumar, D., H. Sjöstrand, S. Bahauddin Alam, J.-M. Palau, and C. De Saint Jean. 2019. Analysis of the prior nuclear data correlation and its effect on the adjustment in Bayesian inference.in International Conference on Nuclear Data for Science and Technology, Beijing, China, May 19-24, 2019.

Lai, D., Liu, W., Gan, T., Liu, K., Chen, Q., 2019. A review of mitigating strategies to improve the thermal environment and thermal comfort in urban outdoor spaces. Sci. Total Environ. 661, 337–353.

Liu, D., Deng, Q., Ren, Z., Zhou, Z., Song, Z., Huang, J., Hu, R., 2020. Variation trends and principal component analysis of nitrogen oxide emissions from motor vehicles in Wuhan City from 2012 to 2017. Sci. Total Environ. 704, 134987.

Liu, L., Song, B., Zhang, S., Liu, X., 2017. A novel principal component analysis method for the reconstruction of leaf reflectance spectra and retrieval of leaf biochemical contents. Remote Sensing 9, 1113.

Liu, Q., G. Liu, C. Huang, S. Liu, and J. Zhao. 2014. A tasseled cap transformation for Landsat 8 OLI TOA reflectance images. Pages 541-544 in Geoscience and Remote Sensing Symposium (IGARSS), 2014 IEEE International. IEEE.

Liu, Q., Liu, G., Huang, C., Xie, C., 2015. Comparison of tasselled cap transformations based on the selective bands of Landsat 8 OLI TOA reflectance images. Int. J. Remote Sens. 36, 417–441.

Liu, Y., Hoppe, B.O., Convertino, M., 2018. Threshold evaluation of emergency risk communication for health risks related to hazardous ambient temperature. Risk Anal. 38, 2208–2221.

Mijani, N., Alavipanah, S.K., Hamzeh, S., Firozjaei, M.K., Arsanjani, J.J., 2019. Modeling thermal comfort in different condition of mind using satellite images: An Ordered Weighted Averaging approach and a case study. Ecol. Ind. 104, 1–12.

Moghaddam, M.H.R., Sedighi, A., Fasihi, S., Firozjaei, M.K., 2018. Effect of environmental policies in combating aeolian desertification over Sejzy Plain of Iran. Aeolian Res. 35, 19–28.

Morris, K.I., Chan, A., Morris, K.J.K., Ooi, M.C., Oozeer, M.Y., Abakr, Y.A., Nadzir, M.S.M., Mohammed, I.Y., Al-Qrimli, H.F., 2017. Impact of urbanization level on the interactions of urban area, the urban climate, and human thermal comfort. Appl. Geogr. 79, 50–72.

Mushore, T.D., Odindi, J., Dube, T., Mutanga, O., 2018. Outdoor thermal discomfort analysis in Harare, Zimbabwe in Southern Africa. S. Afr. Geogr. J. 100, 162–179.

Musse, M.A., Barona, D.A., Rodriguez, L.M.S., 2018. Urban environmental quality assessment using remote sensing and census data. Int. J. Appl. Earth Obs. Geoinf. 71, 95–108.

Otukei, J.R., Blaschke, T., 2010. Land cover change assessment using decision trees, support vector machines and maximum likelihood classification algorithms. Int. J. Appl. Earth Obs. Geoinf. 12, S27–S31.

Panah, S., M. K. Mogaddam, and M. K. Firozjaei. MONITORING SPATIOTEMPORAL CHANGES OF HEAT ISLAND IN BABOL CITY DUE TO LAND USE CHANGES. International Archives of the Photogrammetry, Remote Sensing & Spatial Information Sciences 42 2017.

Potchter, O., Ben-Shalom, H.I., 2013. Urban warming and global warming: Combined effect on thermal discomfort in the desert city of Beer Sheva, Israel. J. Arid Environ. 98, 113–122.

Qaid, A., Lamit, H.B., Ossen, D.R., Shahminan, R.N.R., 2016. Urban heat island and thermal comfort conditions at micro-climate scale in a tropical planned city. Energy Build. 133, 577–595.

Schaffrin, B., Felus, Y.A., 2005. On total least-squares adjustment with constraints. In: A Window on the Future of. Geodesy. Springer, pp. 417–421.

Senanayake, I.P., Welivitiya, W., Nadeeka, P.M., 2013. Remote sensing based analysis of urban heat islands with vegetation cover in Colombo city, Sri Lanka using Landsat-7 ETM+ data. Urban Clim. 5, 19–35.

Silva, J.S., da Silva, R.M., Santos, C.A.G., 2018. Spatiotemporal impact of land use/land cover changes on urban heat islands: A case study of Paço do Lumiar, Brazil. Build. Environ. 136, 279–292.

Sobrino, J.A., Oltra-Carrió, R., Sòria, G., Jiménez-Muñoz, J.C., Franch, B., Hidalgo, V., Mattar, C., Julien, Y., Cuenca, J., Romaguera, M., 2013. Evaluation of the surface urban heat island effect in the city of Madrid by thermal remote sensing. Int. J. Remote Sens. 34, 3177–3192.

Song, Y., Wu, C., 2018. Examining human heat stress with remote sensing technology. GIScience & remote sensing 55, 19–37.

Taleghani, M., 2018. The impact of increasing urban surface albedo on outdoor summer thermal comfort within a university campus. Urban Clim. 24, 175–184.

Taleghani, M., Berardi, U., 2018. The effect of pavement characteristics on pedestrians' thermal comfort in Toronto. Urban Clim. 24, 449–459.

Thom, E.C., 1959. The discomfort index. Weatherwise 12, 57–61.

Toy, S., Yilmaz, S., Yilmaz, H., 2007. Determination of bioclimatic comfort in three different land uses in the city of Erzurum, Turkey. Build. Environ. 42, 1315–1318.

Tsunematsu, N., Yokoyama, H., Honjo, T., Ichihashi, A., Ando, H., Shigyo, N., 2016. Relationship between land use variations and spatiotemporal changes in amounts of thermal infrared energy emitted from urban surfaces in downtown Tokyo on hot summer days. Urban Clim. 17, 67–79.

Tucker, C.J., 1979. Red and photographic infrared linear combinations for monitoring vegetation. Remote Sens. Environ. 8, 127–150.

Van Hove, L., Jacobs, C., Heusinkveld, B., Elbers, J., Van Driel, B., Holtslag, A., 2015. Temporal and spatial variability of urban heat island and thermal comfort within the Rotterdam agglomeration. Build. Environ. 83, 91–103.

Wang, T., Kou, X., Xiong, Y., Mou, P., Wu, J., Ge, J., 2010. Temporal and spatial patterns of NDVI and their relationship to precipitation in the Loess Plateau of China. Int. J. Remote Sens. 31, 1943–1958.

Wang, W., Zhu, L., Wang, R., 2004. An analysis on spatial variation of urban human thermal comfort in Hangzhou, China. Journal of environmental sciences (China) 16, 332–338.

Weng, Q., Firozjaei, M.K., Kiavarz, M., Alavipanah, S.K., Hamzeh, S., 2019. Normalizing land surface temperature for environmental parameters in mountainous and urban areas of a cold semi-arid climate. Sci. Total Environ. 650, 515–529.

P.R. Wolf C.D. Ghilani Adjustment computations: statistics and least squares in surveying and GIS 1997 Wiley-Interscience worldpopulationreview. 2018. http://worldpopulationreview.com.

Xu, H., Hu, X., Guan, H., He, G., 2017. Development of a fine-scale discomfort index map and its application in measuring living environments using remotely-sensed thermal infrared imagery. Energy Build. 150, 598–607.

Yan, L., Roy, D., Li, Z., Zhang, H., Huang, H., 2018. Sentinel-2A multi-temporal misregistration characterization and an orbit-based sub-pixel registration methodology. Remote Sens. Environ. 215, 495–506.

Yang, W., Wong, N.H., Jusuf, S.K., 2013. Thermal comfort in outdoor urban spaces in Singapore. Build. Environ. 59, 426–435.

Yu, X., Guo, X., Wu, Z., 2014. Land surface temperature retrieval from Landsat 8 TIRS—Comparison between radiative transfer equation-based method, split window

algorithm and single channel method. Remote Sensing 6, 9829–9852.

Zha, Y., Gao, J., Ni, S., 2003. Use of normalized difference built-up index in automatically mapping urban areas from TM imagery. Int. J. Remote Sens. 24, 583–594.

Zhang, J., Wang, C.-M., Liu, L., Guo, H., Liu, G.-D., Li, Y.-W., Deng, S.-H., 2014. Investigation of carbon dioxide emission in China by primary component analysis. Sci. Total Environ. 472, 239–247.

Zhang, Y., Odeh, I.O., Han, C., 2009. Bi-temporal characterization of land surface temperature in relation to impervious surface area, NDVI and NDBI, using a sub-pixel image analysis. Int. J. Appl. Earth Obs. Geoinf. 11, 256–264.

Ziaul, S., Pal, S., 2019. Assessing outdoor thermal comfort of English Bazar Municipality and its surrounding, West Bengal, India. Adv. Space Res. 64, 567–580.